Energy performance analysis of a backpack suspension system with a timed clutch for human load carriage

Roee Keren[1], Yizhar Or[2]

[1]*Faculty of Mechanical Engineering, Technion. kroee@tx.technion.ac.il*

[2]*Faculty of Mechanical Engineering, Technion. izi@technion.ac.il*

Abstract

This work theoretically investigates methods of reducing the energetic cost of bipedal walking while carrying a backpack with a suspension system. We extend a previous 2DOF model proposed by Ackerman and Seipel (2014) by adding a timed clutch to the suspension mechanism. The clutch allows the mechanism to switch between states of elastic or rigid connection of the backpack and the body. Periodic switching between the two states of the mechanism is either event-based or timing-based, and may result in inelastic impacts. We study the hybrid dynamics induced by the action of the clutch mechanism, analyze energy expenditure and stability of periodic solutions, and seek for optimal values of stiffness and switching times that minimize the energetic cost. It is found that in many cases, the clutch mechanism can significantly reduce energy expenditure compared to both rigid and elastic suspensions.

1 Introduction

Walking while carrying loads has been a commonly performed task since early human history. Traditional farmers, outdoor hikers, combat soldiers, technical maintenance staff, search-and-rescue and medical crew, are all required to carry heavy loads for long distances [1],[2],[3]. Carrying loads during legged locomotion is an energy consuming task, where the energetic cost is influenced by various factors such as weight, walking speed, and slope [4],[5],[6],[7]. Many attempts have been made to reduce the energetic cost of laden walking, for improving life quality, durability and effectiveness of the various carrying tasks mentioned above. Carrying a load using elastic elements is an ancient strategy, as implemented in the "milkmaid's yoke" and other carrying poles of Asian farmers [8]. Experimental measurements have shown that using carrying poles results in noticeable reduction in muscular loads and ground reaction forces, but not in energy saving [9]. On the other hand, it is known that elastic energy storage in muscles and tendons plays an important role in energy efficiency of animal locomotion [10]. In the recent decades, various systems of elastic suspension for carried backpacks have been developed and tested [11],[12]. Later works have presented theoretical analysis of carrying elastically suspended loads. The work [13] analyzed the influence of elastically-suspended backpack on the dynamic load acting on the body. The recent work of Ackerman and Seipel [14] has presented a simple theoretical model of the

human-backpack dynamics as a two-mass system, where the vertical oscillations of the human's center of mass during walking are actuated by an external harmonic input of "effective leg length". This model has been utilized in [14] in order to analyze the mechanical energy expenditure and comparing it to experimental measurements of backpack suspension systems [11],[12]. It has been found in [14] that the theoretical model analysis can be useful for cleverly choosing suspension system parameters in a way that results in reduction in energy cost of laden walking.

The use of passive elastic elements for assisting legged locomotion has recently become increasingly attractive [15],[16] and particularly the design of wearable devices, either for healthy humans [17],[18],[19], rehabilitation [20],[21],[22] or amputees' prosthetics [23]. These wearable devices often include a combination of springs and timed clutches [18],[19],[24] or brakes [22]. Timed engagement and release of clutches can be utilized in order to disconnect the spring during leg swing [19],[20], trigger a mechanical damper at knee joint [17], or change the foot-ankle impedance during walking gait, from a soft spring to a stiff bumper [25]. The combination of timed clutches and springs induces a multi-modal dynamics for different stages of the periodic gait, and it has been shown that such systems can be designed in clever ways that reduces the overall energetic cost of walking. In spite of the remarkable success of this concept for wearable walking assistance devices, incorporating timed clutch mechanisms into a backpack suspension system has not yet been studied.

The goal of this work is to theoretically study the effect of adding a timed clutch into a backpack suspension system on potential saving in energetic cost. We use the simple model studied in [14], which describes the vertical motion of the human and backpack through a system of two masses connected by springs and dampers and actuated by a harmonic base excitation. The clutch is represented by time-periodic switches between two states of the connection between the masses, from a spring-damper element to a rigid constraint and vice versa. Two possible switching laws are considered. The first law is based purely on timing, and thus it involves an inelastic impact that instantaneously stops the relative motion between masses. The second switching law is based on event detection that locks the connection without impact, when the relative velocity crosses zero. Both switching laws induce hybrid dynamical systems whose solutions involve non-smooth transitions. We find periodic solutions for these systems and analyze their orbital stability. Then we compute the energy expenditure over a non-smooth periodic solution, and study its dependence on switching times of the clutch. We numerically optimize the timing parameters and suspension stiffness, for achieving minimal energetic cost. The theoretical analysis proves that adding the clutch and cleverly choosing its timing can result in significant reduction in energetic cost of laden walking, and also in improving robustness of the suspension system's performance with respect to changes in task conditions such as load and walking speed.

2. Problem statement and formulation

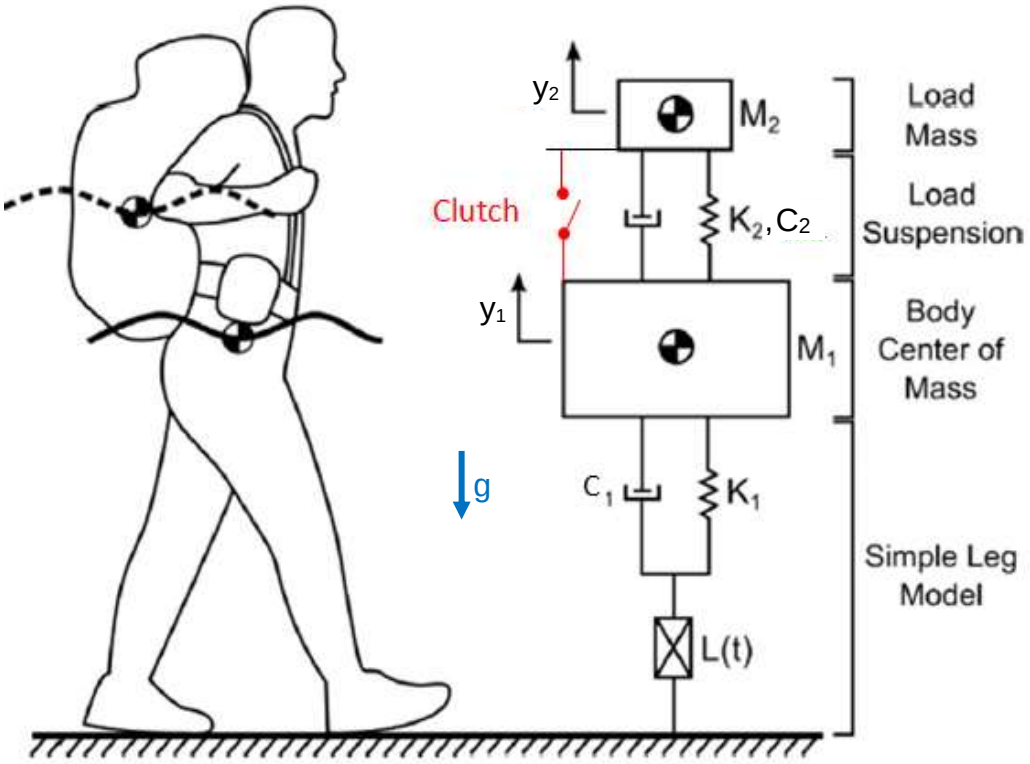

Figure 1: The simple model from [14] of a walker with a suspended backpack

We now review the simplified theoretical model of the backpack suspension system presented by Ackerman and Seipel [14], discuss our addition of a clutch, and formulate the system's dynamic equations. The model in [14] represents the suspension using a two-mass system that move in vertical direction. The model has two degrees of freedom: the vertical translations of the body $y_1(t)$ and of the backpack $y_2(t)$. The masses of the body and the backpack are m_1, m_2, respectively. The dynamics of the legs is represented by [26] linear stiffness k_1 and damping c_1 and a periodically-varying "effective length" $L(t)$, which is regarded as the input of the system. Its value is given as a harmonic function: $L(t) = A\sin(\omega t)$, where the frequency ω is determined from the mean walking speed [27]. The backpack is connected to the body via a suspension system with linear stiffness k_2 and damping c_2. Nominal values of the system's physical parameters, which are taken from [14], appear in Table 1. In particular, values of the suspension system parameters k_2, c_2 are adapted from the experiments in [11]. The dynamic equations of the system are given by:

$$\begin{cases} m_1\ddot{y}_1 + (k_1+k_2)y_1 - k_2y_2 + (c_1+c_2)\dot{y}_1 - c_2\dot{z}_2 = k_1L + c_1\dot{L} - m_1g \\ m_2\ddot{y}_2 - k_2y_1 + k_2y_2 - c_2\dot{y}_1 + c_2\dot{y}_2 = -m_2g \end{cases} \quad (1)$$

Next, we define the variables z_1, z_2 which denote deviations from the nominal equilibrium positions of the system:

(2) $$z_1 = y_1 + \frac{m_1 + m_2}{k_1} g,\ z_2 = y_2 + \frac{m_1 + m_2}{k_1} g + \frac{m_2}{k_2} g$$

Expressing the equations of motion (1) in terms of the variables z_i instead of y_i gives identical equations except for elimination of the gravity forces $m_i g$. These equations can then be written in state-space formulation as:

(3) $$\dot{\mathbf{x}}(t) = \underbrace{\begin{pmatrix} 0 & 1 & 0 & 0 \\ -\frac{k_1 + k_2}{m_1} & -\frac{c_1 + c_2}{m_1} & \frac{k_2}{m_1} & \frac{c_2}{m_1} \\ 0 & 0 & 0 & 1 \\ \frac{k_2}{m_2} & \frac{c_2}{m_2} & -\frac{k_2}{m_2} & -\frac{c_2}{m_2} \end{pmatrix}}_{\mathbf{A}_F} \mathbf{x}(t) + \underbrace{\begin{pmatrix} 0 & 0 \\ \frac{k_1}{m_1} & \frac{c_1}{m_1} \\ 0 & 0 \\ 0 & 0 \end{pmatrix}}_{\mathbf{B}_F} \begin{pmatrix} L(t) \\ \dot{L}(t) \end{pmatrix}$$

Where the state vector is defined as $\mathbf{x}(t) = \begin{pmatrix} z_1 & \dot{z}_1 & z_2 & \dot{z}_2 \end{pmatrix}^T$.

Table 1. Values of physical parameter for the model

Symbol	Name	Value	Symbol	Name	Value
ω	Actuator frequency	11.86 [*rad/s]*	m_1	Body mass	$74[kg]$
k_1	Leg stiffness	$28{,}500[N/m]$	c_1	Leg damping	$950[Ns/m]$
A	Actuator amplitude	$0.01[m]$	g	Gravity acceleration	$9.8[m/s^2]$
m_1	Backpack mass	typically $16[kg]$	T	Cycle period	$0.53[s]$
k_2	Suspension stiffness	$5147[N/m]$	c_2	Suspension damping	$320[Ns/m]$

The *energy expenditure E* of the "effective leg" over a single period of $T = 2\pi/\omega$ is considered in [14] as an important performance measure of the system. This energy expenditure is obtained by integration the mechanical power $P(t)$ at the leg:

(4) $$E = \int_0^T P(t)\,dt = \int_0^T f_L(t)\dot{L}(t)\,dt = \int_0^T \left(k_1(L - z_1) + c_1(\dot{L} - \dot{z}_1) - (m_1 + m_2)g\right)\dot{L}dt$$

It has been shown in [14] that adding the suspension system can lead to significant reduction of *E*.

From this point and on, we consider our extension of the model given in [14]. We add a timed clutch mechanism to lock and release the suspension which connects the body and the backpack. When the clutch is engaged, the velocities of the body and backpack are equal $\dot{z}_1 = \dot{z}_2$, and their relative distance is kept constant. In this state, the system is referred to as 'Locked'. When the clutch is disengaged, there is

no constraint on the relative positions and velocities, which are governed by the spring-damper dynamics. In this state, the system is referred to as 'Free'. While the dynamics of the free system is governed by equation (3), the dynamic equation for the locked system is given by:

$$\dot{\mathbf{x}}(t)=\underbrace{\begin{pmatrix} 0 & 1 & 0 & 0 \\ \frac{-k_1}{m_1+m_2} & \frac{-c_1}{m_1+m_2} & 0 & 0 \\ 0 & 1 & 0 & 0 \\ \frac{-k_1}{m_1+m_2} & \frac{-c_1}{m_1+m_2} & 0 & 0 \end{pmatrix}}_{\mathbf{A}_L}\mathbf{x}(t)+\underbrace{\begin{pmatrix} 0 & 0 \\ \frac{k_1}{m_1+m_2} & \frac{c_1}{m_1+m_2} \\ 0 & 0 \\ \frac{k_1}{m_1+m_2} & \frac{c_1}{m_1+m_2} \end{pmatrix}}_{\mathbf{B}_L}\begin{pmatrix} L(t) \\ \dot{L}(t) \end{pmatrix} \tag{5}$$

Note that locking effectively reduces the dimension of the system in (5) from 4 to 2. Nevertheless, we choose to write (5) in a redundant form using 4x4 matrix for handling the transitions between locked and free states more conveniently.

Switching laws: The clutch mechanism is assumed to switch back and forth between free and locked states once every period *T* of the input $L(t)$. In this work we consider two different switching laws, as follows:

In the *event-based switching law*, locking occurs periodically at a time δ where the backpack-body relative velocity is zero, $\dot{z}_1(\delta)=\dot{z}_2(\delta)$. Thus, no impact occurs at the time of locking. The clutch is released periodically when the input $L(t)$ is at an arbitrary time φ. The *timing-based switching law* still involves release when the input $L(t)$ is at and arbitrary time φ, whereas locking occurs at a time δ which is also chosen arbitrarily. Since the relative velocity $\dot{z}_1(\delta)-\dot{z}_2(\delta)$ at the locking time is not necessarily zero, an *impact* occurs at time $t=\delta$, resulting in discontinuous velocity jump. We assume perfectly inelastic collision, so that the post-impact velocities satisfy $\dot{z}_1^{+}=\dot{z}_2^{+}$. Since the impact is applied internally by the clutch, the total linear momentum is conserved, $(m_1+m_2)\dot{z}_2^{+}=m_1\dot{z}_1^{-}+m_2\dot{z}_2^{-}$. Therefore, the post-impact value of the state vector at time δ^{+} is obtained from its pre-impact value at time δ^{-} as $\mathbf{x}(\delta^{+})=\mathbf{P}\mathbf{x}(\delta^{-})$ where:

$$\underbrace{\begin{pmatrix} z_1^{+} \\ \dot{z}_1^{+} \\ z_2^{+} \\ \dot{z}_2^{+} \end{pmatrix}}_{\mathbf{x}(\delta^{+})}=\underbrace{\begin{pmatrix} 1 & 0 & 0 & 0 \\ 0 & \frac{m_1}{m_1+m_2} & 0 & \frac{m_2}{m_1+m_2} \\ 0 & 0 & 1 & 0 \\ 0 & \frac{m_1}{m_1+m_2} & 0 & \frac{m_2}{m_1+m_2} \end{pmatrix}}_{\mathbf{P}}\underbrace{\begin{pmatrix} z_1^{-} \\ \dot{z}_1^{-} \\ z_2^{-} \\ \dot{z}_2^{-} \end{pmatrix}}_{\mathbf{x}(\delta^{-})} \tag{6}$$

The matrix **P** is called the *impact matrix*. The positions z_1, z_2 are not required to be equal at the moment of impact, and do not change due to the impact. Importantly, the dynamics induced by any of the switching laws is a *hybrid system* composed of

switching between two linear systems, and possibly also a discrete jump in state due to impacts.

3. Analysis of periodic solutions and their stability

In this section, we find periodic solutions of the hybrid system under the two switching laws, and analyze their stability. First, we review the general solution of a linear system of equations under harmonic inputs. Next, we find the possible periodic solutions for the timing-based switching law and the event-based switching law. Finally, we analyze the orbital stability of these periodic solutions

3.1 Review on solutions of linear systems under harmonic inputs.

Given a linear system $\dot{\mathbf{x}}(t)=\mathbf{A}\mathbf{x}(t)+\mathbf{B}\mathbf{u}(t)$ where $\mathbf{u}(t)=\left(L(t),\ \dot{L}(t)\right)^T$ the solution $\mathbf{x}(t)$ under initial condition $\mathbf{x}(t_0)=\mathbf{x}_0$ is a superposition of steady-state and transient solutions $\mathbf{x}(t)=\mathbf{s}(t)+\mathbf{r}(t)$. The steady-state solution is the frequency response to the harmonic inputs:

(7) $$\mathbf{s}(t)=\mathbf{v}\cos(\omega t)+\mathbf{w}\sin(\omega t).$$

The constant vectors $\mathbf{v},\mathbf{w}$ depend on **A**,**B** and on ω. The transient solution is

(8) $$\mathbf{r}(t)=e^{\mathbf{A}(t-t_0)}\left(\mathbf{x}_0-\mathbf{s}(t_0)\right),$$

where the matrix exponential in (8) is defined as the converging infinite sum:

$$e^{\mathbf{A}t}=\mathbf{I}+\mathbf{A}t+\frac{1}{2}(\mathbf{A}t)^2+\ldots+\frac{1}{n!}(\mathbf{A}t)^n+\ldots$$

The exponent can be expressed in closed form using the eigenvalues λ_i of $\mathbf{A}$ [28]. For example, it can be obtained from the relation $e^{\mathbf{A}t}=\mathbf{M}^{-1}e^{\Lambda t}\mathbf{M}$, where $\mathbf{\Lambda}$, is a diagonal matrix containing the eigenvalues of **A** and **M** is a matrix whose columns are eigenvectors of $\mathbf{A}$. The two systems, free and locked, have different **A**,**B** matrices in (3) and (5), denoted as $\mathbf{A}_F,\mathbf{B}_F$ and $\mathbf{A}_L,\mathbf{B}_L$. The steady state and transient responses of the systems will also be denoted with subscripts: F-free or L-locked, as $\mathbf{r}_F,\mathbf{s}_F,\mathbf{r}_L,\mathbf{s}_L$. For convenience, we exploit the time-invariance of the system and of the periodic input $L(t)$, and shift the time by φ such that the clutch release occurs at $t=0$ for both switching laws, while the input's time is shifted as $L(t)\to L(t+\varphi)=A\sin\left(\omega(t+\varphi)\right)$. The locking time δ now expresses the *duration* of released state of the clutch in a single period.

3.2 Periodic solutions under the timing-based switching law

We now find periodic solutions under the timing-based switching law. We consider only *synchronous solutions* which have the same period as the input signal, $T=\frac{2\pi}{\omega}$.

According to (3),(7),(8), the solution at times $0<t<\delta$ is:

(9) $$\mathbf{x}(t)=e^{\mathbf{A}_F t}\left(\mathbf{x}_0-\mathbf{s}_F(\varphi)\right)+\mathbf{s}_F(t+\varphi),\quad 0<t<\delta$$

Note that the steady-state solution in (9) is time-shifted due to our choice to use the shifted input $L(t+\varphi)$. At time t=δ, the clutch locks and an impact occurs. According to (6) and (9), the system's state right after locking is:

(10) $$\mathbf{x}(\delta^+) = \mathbf{P}\left(e^{\mathbf{A}_F\delta}\left(\mathbf{x}_0 - \mathbf{s}_F(\varphi)\right) + \mathbf{s}_F(\delta+\varphi)\right)$$

Using (5)-(8),(10), the system's solution for times $\delta < t \le T$ when the system is locked is given by:

(11)
$$\begin{aligned}\mathbf{x}(t) &= e^{\mathbf{A}_L(t-\delta)}\left(\mathbf{x}(\delta^+) - \mathbf{s}_L(\delta+\varphi)\right) + \mathbf{s}_L(t+\varphi) \\ &= e^{\mathbf{A}_L(t-\delta)}\left(\mathbf{P}\left(e^{\mathbf{A}_F\delta}\left(\mathbf{x}_0 - \mathbf{s}_F(\varphi)\right) + \mathbf{s}_F(\delta+\varphi)\right) - \mathbf{s}_L(\delta+\varphi)\right) + \mathbf{s}_L(t+\varphi)\end{aligned}$$

Substituting t=T into (11) and using the periodicity of $\mathbf{s}_L(t)$, the system's state at the end of the period is given by:

(12) $$\mathbf{x}(T) = e^{\mathbf{A}_L(T-\delta)}\left(\mathbf{P}\left(e^{\mathbf{A}_F\delta}\left(\mathbf{x}_0 - \mathbf{s}_F(\varphi)\right) + \mathbf{s}_F(\delta+\varphi)\right) - \mathbf{s}_L(\delta+\varphi)\right) + \mathbf{s}_L(\varphi)$$

Next, we substitute the requirement $\mathbf{x}(T) = \mathbf{x}_0$ into (12) and get:

(13)
$$\underbrace{\left(\mathbf{I} - e^{\mathbf{A}_L(t-\delta)}\mathbf{P}e^{\mathbf{A}_F\delta}\right)}_{\mathbf{R}(\delta)}\mathbf{x}_0 = \underbrace{e^{\mathbf{A}_L(t-\delta)}\left(\mathbf{P}\left(\mathbf{s}_F(\delta+\varphi) - e^{\mathbf{A}_F\delta}\mathbf{s}_F(\varphi)\right) - \mathbf{s}_L(\delta+\varphi)\right) + \mathbf{s}_L(\varphi)}_{\mathbf{q}(\delta,\varphi)}$$

The initial condition $\mathbf{x}_0$ which results in periodic solution is then obtained as:

(14) $$\mathbf{x}_0 = \mathbf{R}(\delta)^{-1}\mathbf{q}(\delta,\varphi)\ .$$

An example of a (time-shifted) periodic solution under timing-based switching law with $\varphi = 0.32T, \delta = 0.48T$ is shown in Figure 2.

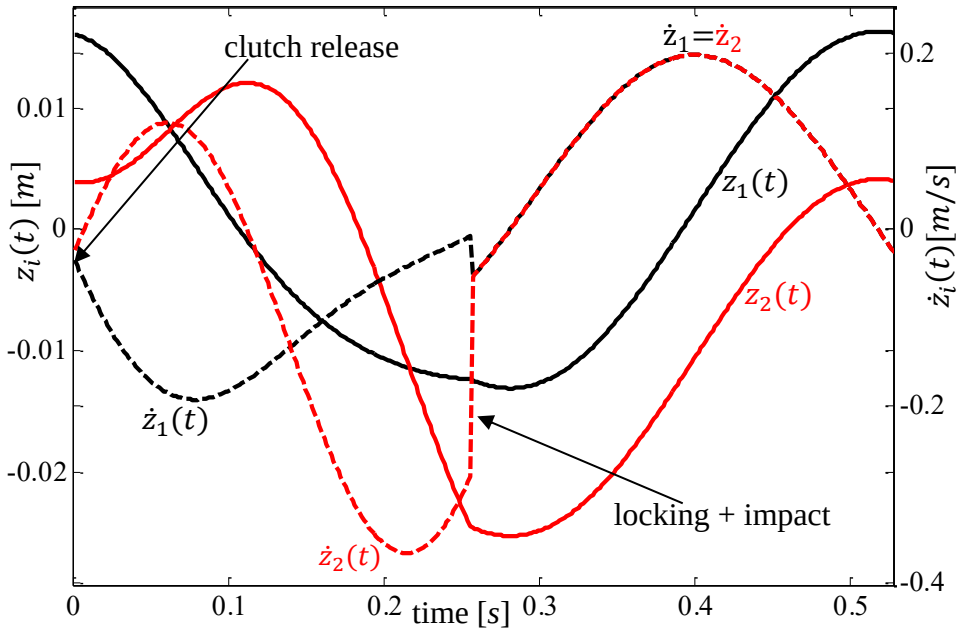

Figure 2: example of a periodic solution under timing-based switching law

3.3 Periodic solution under the event-based switching law

We now compute periodic solutions under the timing-based switching law. In this case, for any choice of the release time φ, the duration δ of released state is determined according to the requirement of zero relative velocity at locking. For convenience, we solve the *inverse problem*, of finding φ under a given choice of δ. First, we use equations (13) and (14), with exclusion of the impact matrix **P**. This gives:

$$(15)\quad \underbrace{\left(\mathbf{I}-e^{\mathbf{A}_L(t-\delta)}e^{\mathbf{A}_F\delta}\right)}_{\tilde{\mathbf{R}}(\delta)}\mathbf{x}_0=\underbrace{e^{\mathbf{A}_L(t-\delta)}\left(\mathbf{s}_F\left(\delta+\varphi\right)-e^{\mathbf{A}_F\delta}\mathbf{s}_F\left(\varphi\right)-\mathbf{s}_L\left(\delta+\varphi\right)\right)+\mathbf{s}_L\left(\varphi\right)}_{\tilde{\mathbf{q}}(\delta,\varphi)}$$

The relation between δ and φ is obtained from the additional requirement of zero-impact switching, $\dot{z}_1(\delta)=\dot{z}_1(\delta)$. According to the dynamics of the locked state in (5), this is equivalent to $\dot{z}_1(T)=\dot{z}_1(T)$, and due to periodicity of the solution, this requirement can be made at the initial time t=0, which gives:

$$(16)\quad \mathbf{H}\mathbf{x}_0=\mathbf{H}\tilde{\mathbf{R}}\left(\delta\right)^{-1}\tilde{\mathbf{q}}\left(\delta,\varphi\right)=0,\ \text{ where } \mathbf{H}=\begin{bmatrix}0 & 1 & 0 & -1\end{bmatrix}.$$

The constraint in (16) can be simplified into a scalar equation in δ,φ as:

$$a(\delta)\cos\left(\omega\varphi\right)+b(\delta)\sin\left(\omega\varphi\right)+c(\delta)\cos\left(\omega\left(\delta+\varphi\right)\right)+d(\delta)\sin\left(\omega\left(\delta+\varphi\right)\right)=0$$

$$(17)\quad \begin{aligned}
&\text{where } a(\delta)=\mathbf{H}\left(e^{\mathbf{A}_L(\delta-T)}-e^{\mathbf{A}_F\delta}\right)^{-1}\left(e^{\mathbf{A}_L(\delta-T)}\mathbf{w}_L-e^{\mathbf{A}_F\delta}\mathbf{w}_F\right)\\
&b(\delta)=\mathbf{H}\left(e^{\mathbf{A}_L(\delta-T)}-e^{\mathbf{A}_F\delta}\right)^{-1}\left(e^{\mathbf{A}_L(\delta-T)}\mathbf{v}_L-e^{\mathbf{A}_F\delta}\mathbf{v}_F\right)\\
&c(\delta)=\mathbf{H}\left(e^{\mathbf{A}_L(\delta-T)}-e^{\mathbf{A}_F\delta}\right)^{-1}\left(\mathbf{w}_F-\mathbf{w}_L\right)\\
&d(\delta)=\mathbf{H}\left(e^{\mathbf{A}_L(\delta-T)}-e^{\mathbf{A}_F\delta}\right)^{-1}\left(\mathbf{v}_F-\mathbf{v}_L\right)
\end{aligned}$$

Figure 3. Plots the two solutions of normalized release time φ/T as a function of normalized duration of clutch release δ/T, for satisfying a zero-impact periodic solution from (16). It can be easily verified that for a given choice of δ, there are two solutions for φ which differ by half-period T/2, corresponding to the negated periodic solution under half-period time shift, i.e. **x**(t)→-**x**(t+T/2). On the other hand, for a given choice of φ the two solutions for δ do not differ by half period, and correspond to different periodic solutions. As an example, Figure 4 shows a time plot of the state variables **x**(t) under a zero-impact periodic solution due to event-based switching of the clutch, for $\varphi=0.37T,\delta=0.59T$ (this point is marked by 'x' in Figure 3). Importantly, note that the condition $\dot{z}_1(t)=\dot{z}_2(t)$ occurs *twice* during the periodic solution but locking the clutch occurs only at the *second* crossing event. Thus, deciding which event activates the clutch is determined uniquely by the zero-crossing *direction* of the threshold function $\dot{z}_1(t)-\dot{z}_2(t)$. The two solution branches of (16) in Figure 3 are actually distinguished by different signs of zero-crossing directions.

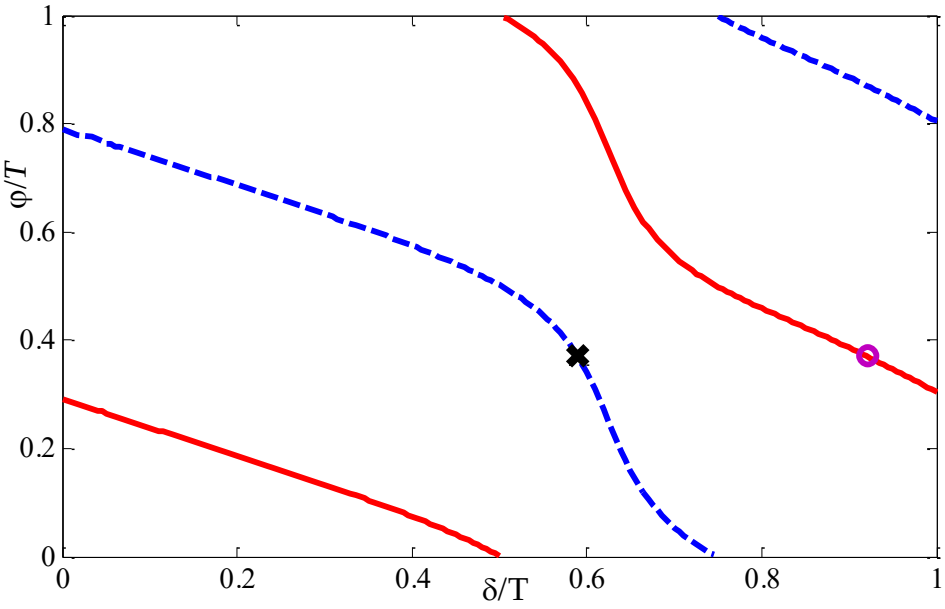

Figure 3: Plot of solutions of (16), switching times φ vs δ that correspond to zero-impact periodic solutions under event-based switching

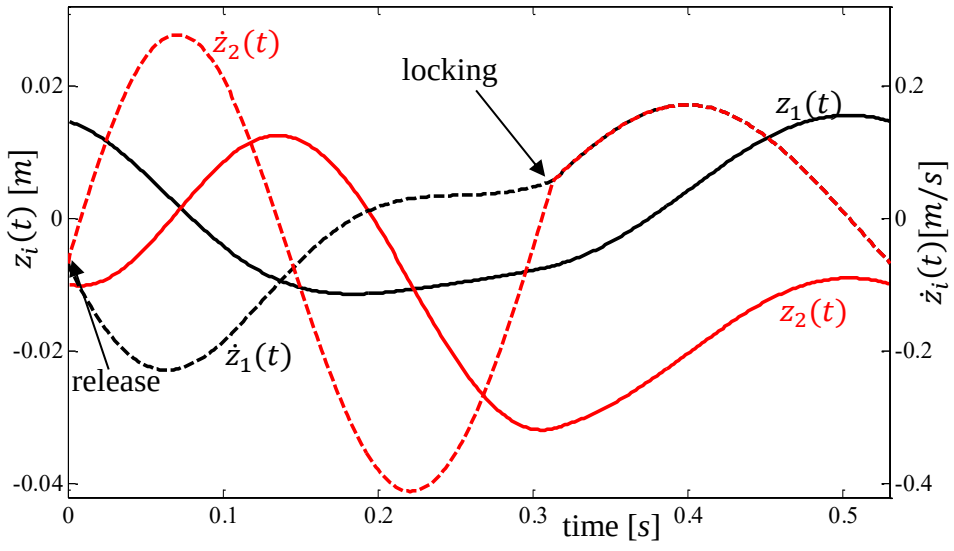

Figure 4: Time plot of a periodic solution with event-based switching (no impact)

3.4 Orbital stability of periodic solutions

In this part, we study the local orbital stability of periodic solutions (cf. [29]). We show either analytically or numerically that the periodic solutions under both switching laws are locally orbitally stable. The stability of periodic solution of the hybrid dynamical system is analyzed as follows. First, we define $\mathbf{x}_k = \mathbf{x}(kT)$, $k = 0,1,2...$, which is the discrete sequence of the system's states at the beginning of each period. The discrete-time dynamics of the system is denoted by the Poincaré map $\mathbf{x}_{k+1} = \mathbf{F}(\mathbf{x}_k)$. A periodic solution of the hybrid system is an initial state $\mathbf{x}_0$

satisfying $\mathbf{x}_0 = \mathbf{F}(\mathbf{x}_0)$, i.e. a fixed point of the Poincaré map **F**. The (local) orbital stability of the periodic solution is determined by the eigenvalues of the Jacobian matrix $\mathbf{J} = \left.\frac{d\mathbf{F}}{d\mathbf{x}}\right|_{\mathbf{x}=\mathbf{x}_0}$. The periodic solution is orbitally stable if and only if all its eigenvalues $\lambda_i(\mathbf{J})$ satisfy $|\lambda_i(\mathbf{J})| < 1$. An equivalent formulation of this stability condition is given by the requirement $\rho(\mathbf{J})<1$, where $\rho(\mathbf{J})$ is the *spectral radius* of **J**, defined as $\rho(\mathbf{J})=\max\{|\lambda_i(\mathbf{J})|\}$.

First, we consider stability of periodic solutions under the timing-based switching law. In this case, the discrete-time map **F** is given explicitly in (12), where $\mathbf{x}(T)$ is given as a function of initial state $\mathbf{x}_0$. Jacobian matrix of **F** is simply obtained as

$$\mathbf{J} = \frac{d\mathbf{x}(T)}{d\mathbf{x}_0} = e^{\mathbf{A}_L(T-\delta)}\mathbf{P}e^{\mathbf{A}_F\delta}. \tag{18}$$

The linear system (3) is stable for any positive values of stiffness and damping k_i, c_i. Therefore, all eigenvalues of $\mathbf{A}_F$ have negative real part. This implies that $\rho(e^{\mathbf{A}_F\delta}) < 1$ for all δ>0, whereas the limiting case of $\delta \to 0$ implies $\rho(e^{\mathbf{A}_F\delta}) \to 1$. In addition, it can be verified from (6) that **P** is a singular matrix whose eigenvalues are {0,1,1,1}. Finally, the matrix $\mathbf{A}_L$ in (5) is of rank 2, and has two zero eigenvalues and two other eigenvalues with negative real part, implying that $\rho(e^{\mathbf{A}_L(T-\delta)}) = 1$ for all δ. We now invoke a known property of spectral radius of a product of matrices (which stems directly from Gelfand's formula [30]), that gives the bound

$$\rho(\mathbf{J}) \le \rho(e^{\mathbf{A}_L(T-\delta)}) \cdot \rho(\mathbf{P}) \cdot \rho(e^{\mathbf{A}_F\delta}). \tag{19}$$

Using the inequality (19), one concludes that $\rho(\mathbf{J}) < 1$ for all δ>0, and thus the periodic solution is stable. The limit case δ=0 corresponds to the locked system (5) without switching, and its "neutral stability" $\rho(\mathbf{J}) = 1$ is due to reduction of the system's effective dimension from 4 to 2. Moreover, since **P** is singular, (20) implies that **J** always has one zero eigenvalue. This is because at the times $t=kT$, the system's state must satisfy the constraint $\dot{z}_1=\dot{z}_2$ which reduces the dimension of the Poincaré section, i.e. the domain and range of **F**, from 4 to 3 (cf. [31],[32]).

Figure 5 plots the response of $\dot{z}_i(t)$ with the timing-based switching law, under a specific initial perturbation from the nominal periodic solution in Figure 2, where the initial velocities are reversed, i.e $\dot{z}_i(0) \to -\dot{z}_i(0)$. The locking (impact) times are denoted by 'x' while the release times are denoted by 'o'. It can be that the solution quickly converges to the nominal periodic solution that appears in Figure 2 (spectral radius for this periodic solution is ρ(**J**)=0.21).

Next, we study the local orbital stability of periodic solutions under the timing-based switching law. Chosen values of φ and δ that solve (16) correspond to a periodic solution with initial state $\mathbf{x}_0$ satisfying (13). When the initial state $\mathbf{x}_0$ is perturbed, the release timing remains at φ, whereas the event-driven locking times change. We denote the discrete sequence of locking times as δ_k, which satisfy the condition $\dot{z}_1(kT + \delta_k) = \dot{z}_2(kT + \delta_k)$. We shift the time by φ as above, so that the release times are at $t=kT$. Using (12) and (16) while excluding the impact matrix **P**,

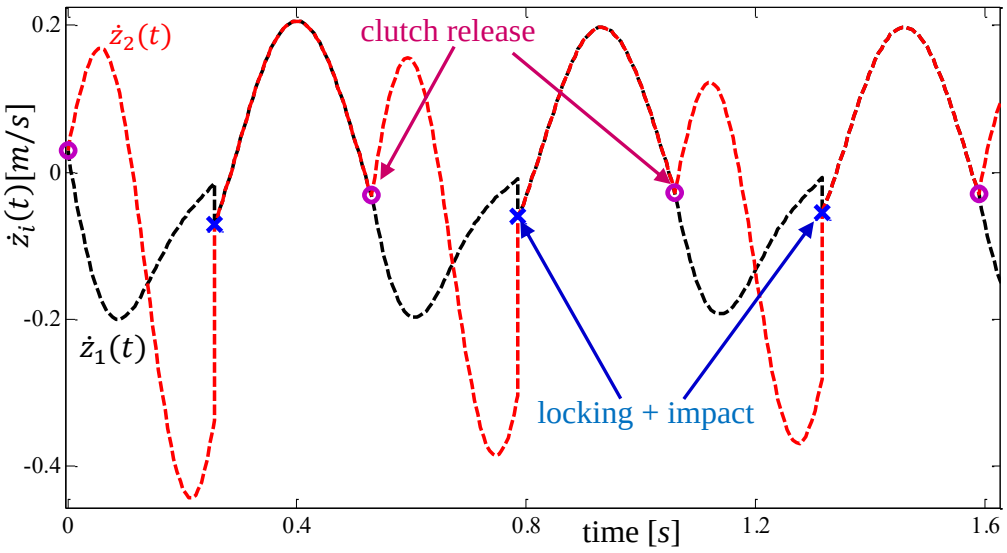

Figure 5: Convergence to the periodic solution with timing-based switching

the discrete-time dynamics of $\mathbf{x}_k = \mathbf{x}(kT)$, combined with the implicit condition for δ_k, are written as:

$$(21)\qquad \begin{cases} \mathbf{x}_{k+1} = e^{\mathbf{A}_L(T-\delta_k)}\left(e^{\mathbf{A}_F\delta_k}\left(\mathbf{x}_k - \mathbf{s}_F(\varphi)\right) + \mathbf{s}_F(\delta_k+\varphi) - \mathbf{s}_L(\delta_k+\varphi)\right) + \mathbf{s}_L(\varphi) \\ f(\mathbf{x}_k,\delta_k) = \mathbf{H}\left(e^{\mathbf{A}_F\delta_k}\left(\mathbf{x}_k - \mathbf{s}_F(\varphi)\right) + \mathbf{s}_F(\delta_k+\varphi)\right) = 0 \end{cases}$$

The Jacobian matrix **J** can then be obtained as

$$(22)\qquad \mathbf{J} = \left.\frac{d\mathbf{x}_{k+1}(\mathbf{x}_k,\delta_k)}{d\mathbf{x}_k}\right|_* = \left.\frac{\partial \mathbf{x}_{\mathbf{x}_{k+1}}}{\partial \mathbf{x}_k}\right|_* + \left.\frac{\partial \mathbf{x}_{\mathbf{x}_{k+1}}}{\partial \delta_k}\frac{\partial \delta_k}{\partial \mathbf{x}_k}\right|_*,$$

where '*' notation means that derivatives are evaluated at the nominal periodic solution, $\mathbf{x}_k = \mathbf{x}_0$, $\delta_k = \delta$ and the chosen value of φ. The partial derivatives of $\mathbf{x}_{k+1}$ in (19) are obtained directly from (21) as:

$$(23)\qquad \begin{aligned} \left.\frac{\partial \mathbf{x}_{\mathbf{x}_{k+1}}}{\partial \mathbf{x}_k}\right|_* &= e^{\mathbf{A}_L(T-\delta)}e^{\mathbf{A}_F\delta}, \\ \left.\frac{\partial \mathbf{x}_{\mathbf{x}_{k+1}}}{\partial \delta_k}\right|_* &= \left(\mathbf{A}_F - \mathbf{A}_L\right)e^{\mathbf{A}_L(T-\delta)}e^{\mathbf{A}_F\delta}\left(\mathbf{x}_k - \mathbf{s}_F(\varphi)\right) - \mathbf{A}_L\left(\mathbf{s}_F(\delta+\varphi) - \mathbf{s}_L(\delta+\varphi)\right), \\ &\quad + e^{\mathbf{A}_L(T-\delta)}\left(\dot{\mathbf{s}}_F(\delta+\varphi) - \dot{\mathbf{s}}_L(\delta+\varphi)\right) \end{aligned}$$

The derivative of δ_k in (19) is obtained by differentiation of the implicit constraint $f(\mathbf{x}_k,\delta_k) = 0$ in (18) as:

$$(24)\qquad \begin{aligned} &\frac{\partial f}{\partial \mathbf{x}_k} + \frac{\partial f}{\partial \delta_k}\frac{\partial \delta_k}{\partial \mathbf{x}_k} = 0 \;\Rightarrow\; \left.\frac{\partial \delta_k}{\partial \mathbf{x}_k}\right|_* = -\left(\frac{\partial f}{\partial \delta_k}\right)^{-1}\left.\frac{\partial f}{\partial \mathbf{x}_k}\right|_* \\ &\left.\frac{\partial \delta_k}{\partial \mathbf{x}_k}\right|_* = -\left[\mathbf{H}\left(\mathbf{A}_F e^{\mathbf{A}_F\delta}\left(\mathbf{x}_k - \mathbf{s}_F(\varphi)\right) + \dot{\mathbf{s}}_F(\delta+\varphi)\right)\right]^{-1}\mathbf{H}e^{\mathbf{A}_F\delta} \end{aligned}$$

The Jacobian matrix **J** is then obtained by substituting (23) and (24) into (22). Due to the complexity of **J**, its eigenvalues can be computed only numerically. Figure 6 plots the absolute values $|\lambda_i|$ for the zero-impact periodic solutions as a function of

the normalized release duration δ/T. It can be seen that $|\lambda_i| < 1$ and the periodic solution is always orbitally stable for $\delta > 0$. In the limit of $\delta \to 0$, one eigenvalue approaches unity, and the solution becomes marginally stable. This is because the case of $\delta = 0$ represents the fully-locked system in (4), whose effective dimension drops to 2. The plot in Figure 6 also indicates that **J** always has one zero eigenvalue. As explained above, this holds because any small initial perturbation that satisfies $\dot{z}_1(0) \neq \dot{z}_2(0)$ will be suppressed immediately after the first period, due to locking of the clutch.

As a simulation example, Figure 7 plots the response of $\dot{z}_i(t)$ with the event-based switching law and release phase of φ=0.37T, under a specific initial perturbation from the nominal periodic solution in Figure 4, where the initial velocities are reversed, i.e. $\dot{z}_i(0) \to -\dot{z}_i(0)$. The locking (impact) times are denoted by 'x' while the release times are denoted by 'o'. It can be seen that the solution converges to the nominal periodic solution with δ=0.59T that appears in Figure 4 (spectral radius for this periodic solution is ρ(**J**)=0.53). Importantly, this simulation assumes that the switching law for clutch locking is based not only on detecting the event where $\dot{z}_1(t) = \dot{z}_2(t)$, but also on the *direction* of crossing this event, which in our case means that $\dot{z}_1(t^-) > \dot{z}_2(t^-)$. Next, Figure 8 plots the response of $\dot{z}_i(t)$ with the event-based switching law under the *same* initial perturbation, where the switching law is now based on crossing the event in *opposite direction*, i.e. $\dot{z}_1(t^-) < \dot{z}_2(t^-)$. It can be seen that the response converges to a different periodic solution, which is precisely the second solution of δ=0.92T under the same value of φ=0.37T. This solution is marked by 'o' on the solution curves of eq. (16) in Figure 3.

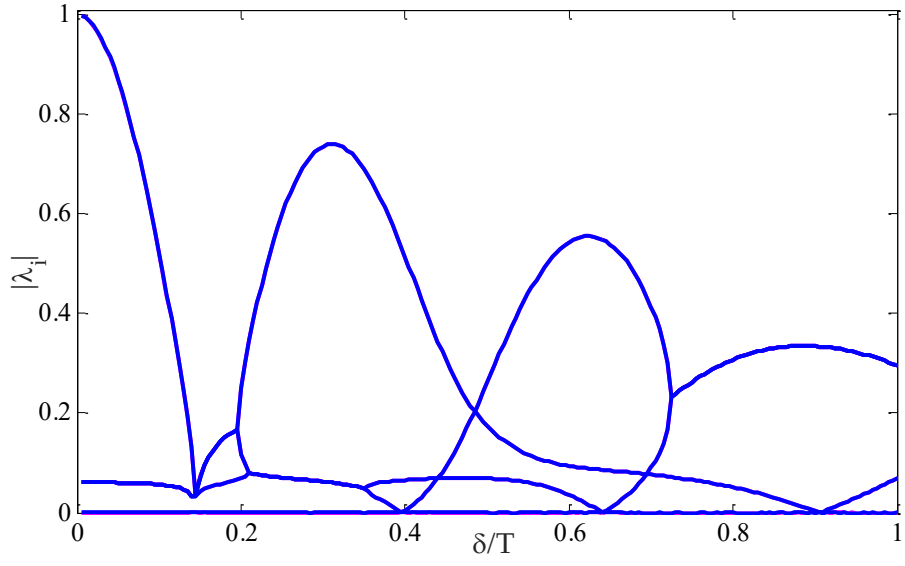

Figure 6: Magnitude of eigenvalues of J under the event-based switching law, as a function of normalized release duration δ/T.

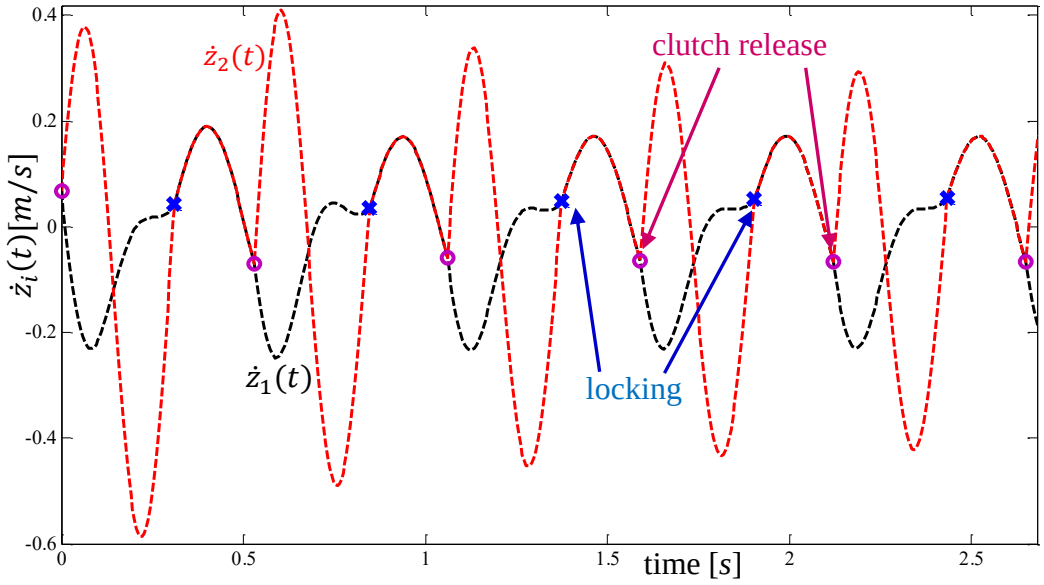

Figure 7: Convergence to the periodic solution with timing-based switching

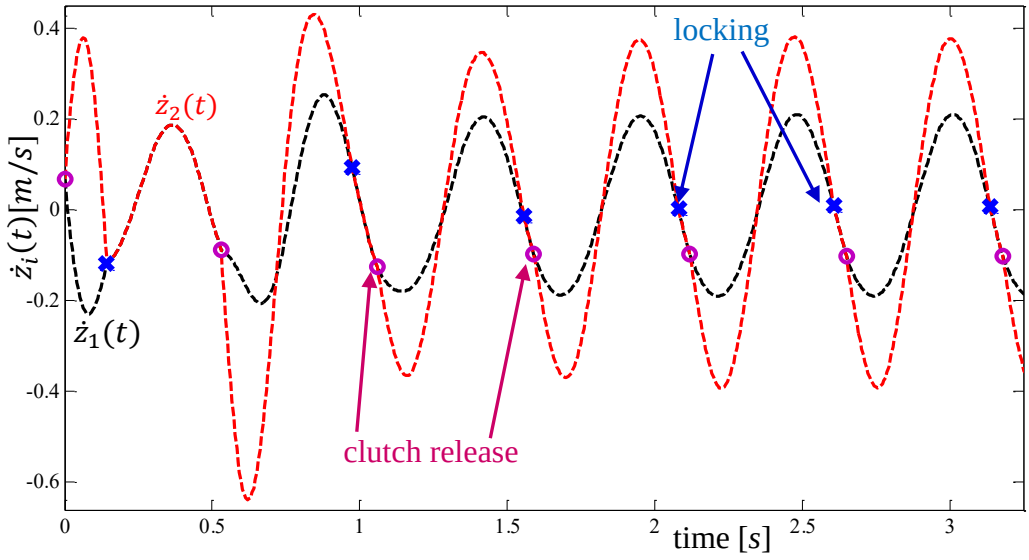

Figure 8: Convergence to a different periodic solution with timing-based switching and opposite direction of event crossing.

4. Energy expenditure and Optimization

In this section, we study optimization of the clutch timing and suspension stiffness in order to minimize the energy expenditure E, which is defined in equation (4). In the previous study in [14] of suspension system without a clutch whose dynamics is governed by the linear system (3), one could readily obtain a closed-form expression for E. This is because the steady-state solution of a linear system under harmonic inputs consists only of harmonic functions at the same frequency, and the mechanical power $P(t)$ can be integrated explicitly. This is not the case in our hybrid system which switches between two linear systems, where the periodic solution also involves transient terms that contain time-exponential functions associated with the

eigenvalues of both $\mathbf{A}_L$ and $\mathbf{A}_F$. A closed-form expression for E thus becomes very cumbersome. Therefore, we focus here on numerical analysis of periodic solutions of the spring-clutch-masses system under both switching laws, aiming at minimization of the energy expenditure E. We first study optimization of the switching times of the clutch, and then also study optimization with respect to stiffness of the suspension system.

4.1 Optimization of clutch timing

We now conduct numerical optimization of the switching times of the clutch under both switching laws, for the nominal parameter values of the suspension system as given in Table 1. We first consider the event-based switching law, where each choice of the release duration δ is associated with two possible solutions for the release time φ which satisfy the zero-impact condition in (15). As explained in Section 3, these two solutions are symmetric and thus result is equal energy expenditure E. Figure 9 plots the energy expenditure E as a function of δ/T under the event-based switching law, which has been obtained via numerical integration of (4) along the periodic solution. It can be seen that there exists an optimal value of $\delta \approx 0.499T$, for which the energy expenditure E is minimized. This optimal clutch timing results in 40% energy saving compared to the case of a free spring ($\delta \to T$), and in 7.6% saving compared to the case of a rigid connection ($\delta \to 0$). Another interesting finding from Figure 9 is the existence of a strong maximum in energy at $\delta \approx 0.65$. This indicates that tuning the correct clutch timing can be very sensitive in terms of energy expenditure.

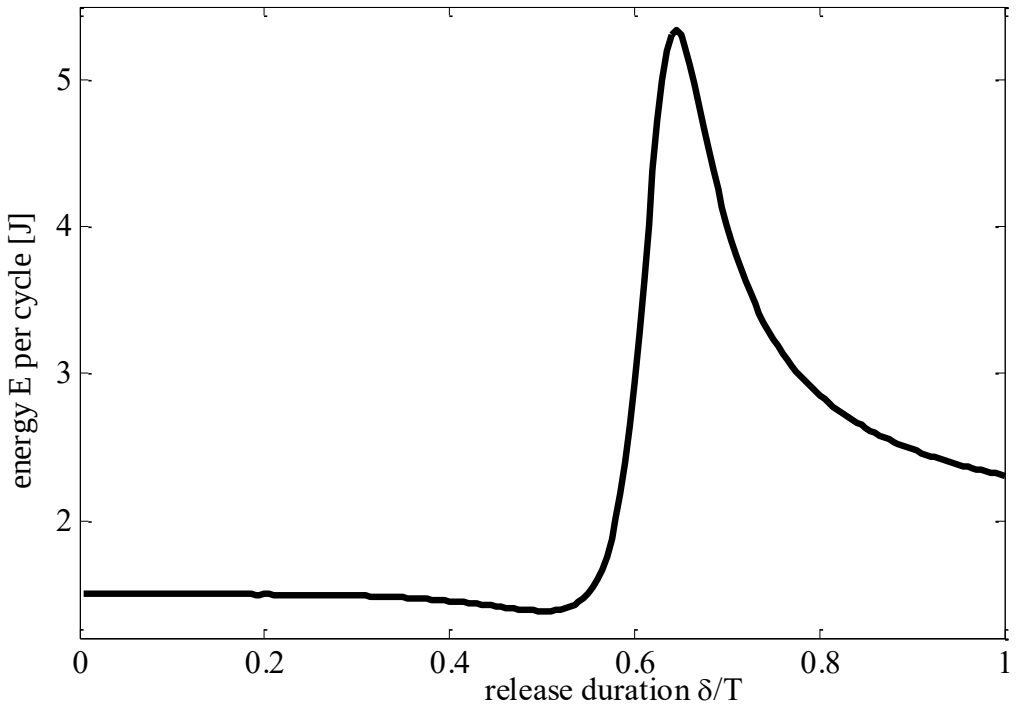

Figure 9: Energy expenditure E as a function of normalized release duration δ/T under the event-based switching law.

Next, we consider the timing-based switching law, where both times δ and φ can be varied. Figure 10 plots a contour plot of the energy level E as a function of δ and φ. Obviously, the energy level is $T/2$-periodic in the release time φ. The maximum points are denoted by 'o' while minimum points are denoted by '+'. The solid thick curves denote combinations of δ and φ associated with zero-impact periodic solutions. That is, these are the solutions of (16), which are also shown in Figure 3. In order to demonstrate the influence of impacts on the energy expenditure, we now consider two sections of the energy contour, for constant value of either δ or φ. Figure 11 shows the energy level as a function of φ/T for $\delta=0.617T$. This is a section of the contour plot in Figure 10 along the vertical dashed line. The plot in Figure 11, which is $T/2$-periodic in φ, shows that minimal energy expenditure is obtained at $\varphi\approx\{0.44T,0.94T\}$, whereas zero impact is obtained at $\varphi\approx\{0.28T,0.78T\}$ (marked by triangles). This shows that (constrained) minimal energy is not necessarily associated with zero impact. On the other hand, Figure 12 plots the energy level as a function of δ/T for $\varphi=0.6T$. This is a section of the contour plot in Figure 10 along the horizontal dashed line. The plot in Figure 12 shows that minimal energy expenditure E is obtained at a $\delta=0.36T$. Moreover, it shows that both minimum and maximum values of E are obtained at zero-impact values of φ (marked by triangles). That is, in this direction of constrained minimization of E under fixed value of δ, the optimum is obtained at zero-impact periodic solutions. This implies that the *global* (unconstrained) optimum of E is also obtained at zero-impact periodic solutions. This optimum is in fact identical to the one obtained under the event-based switching law, as shown in Figure 9 (which is essentially a curved section of the contour plot in Figure 10 along the zero-impact curve).

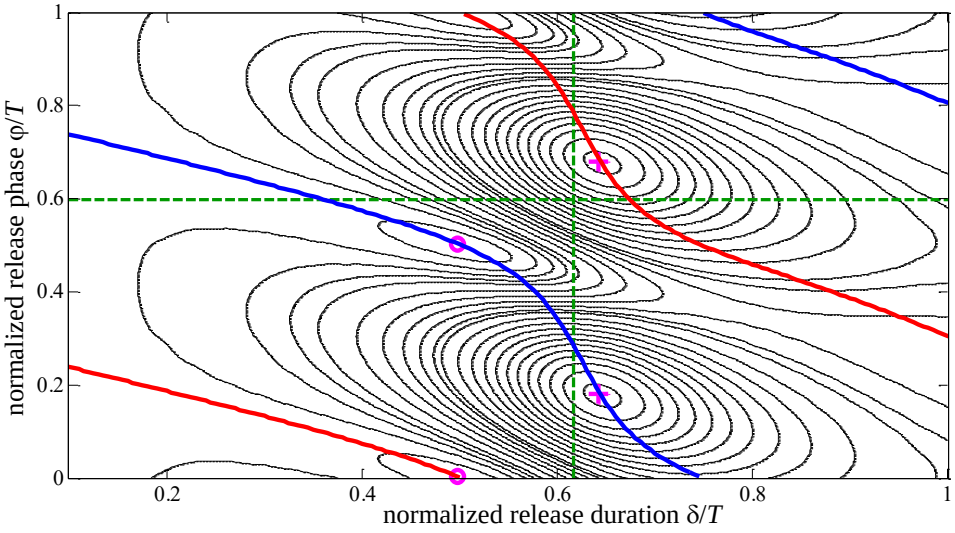

Figure 10: Contour plot of Energy expenditure E as a function of δ/T and φ/T under the timing-based switching law.

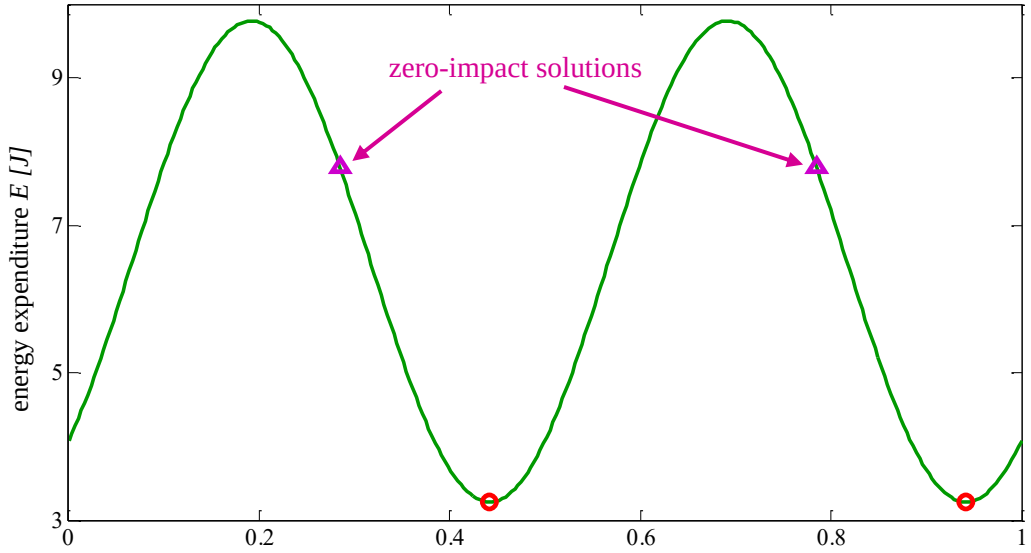

Figure 11: Plot of energy expenditure *E* as a function of φ/*T* for δ=0.617*T* under the timing-based switching law.

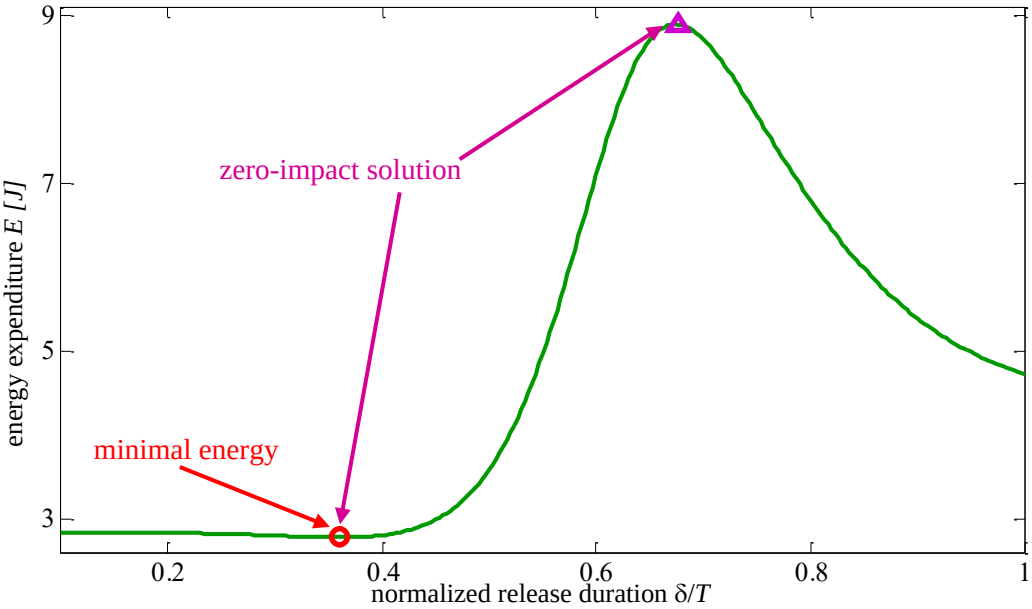

Figure 12: Plot of energy expenditure *E* as a function of δ/*T* for φ=0.6*T* under the timing-based switching law.

Next, we compare the energy performance with two alternative measures of energy expenditure, associated with metabolic cost [33],[34]. The first measure, which has been used in [33] considers only positive work:

$$E_+ = \int_0^T P_+(t)\,dt, \text{ where } P_+(t) = \begin{cases} P(t) & \text{if } P(t) > 0 \\ 0 & \text{otherwise} \end{cases} \tag{25}$$

The second measure, which is used in [34] is based on "metabolic efficiencies" of Margaria [35] that represent muscular work:

$$E_{met} = \int_0^T \frac{P(t)}{\eta(t)}\,dt, \text{ where } \eta(t) = \begin{cases} \eta_+ & \text{if } P(t) > 0 \\ \eta_- & \text{otherwise} \end{cases} \tag{26}$$

The values of the two efficiencies are given in [35] as $\eta_+ = 0.25$ and $\eta_- = -1.2$, where the negative value of η_- reflects the fact that the muscles have to expend positive work in order to absorb negative mechanical energy. Figure 13 plots the two energy measures E_+ and E_{met} as a function of the normalized release duration δ/T under the event-based switching law. For better visibility of the plot, different constant values are subtracted from each energy measure. It can be seen that the mean value of E_+ is larger than that of the mechanical energy E in Figure 9 since only positive energy is counted in (25). The mean value of the metabolic energy E_{met} is about 3-4 times larger than that of E_+ due to dividing by the efficiencies in (26). In addition, recall that for each value of δ, the zero-impact condition (17) has two solutions for φ which correspond to two periodic solutions with phase difference of $T/2$. An interesting difference of the energy measures E_+ and E_{met} from the mechanical energy E in (4) is the fact that the two periodic solutions for a given value of δ give rise to different energy values due to asymmetry of the mechanical power $P(t)$ with respect to zero. Therefore, the energy measures E_+ and E_{met} both have two branches as a function of δ in Figure 13. Comparing to Figure 9, it can be seen that all energy measures for all branches of zero-impact periodic solutions have similar characteristics of an optimal value of δ with minimal energy, followed by a maximal energy at a larger value of δ, whereas the exact values vary depending on the choice of energy measure and periodic solution.

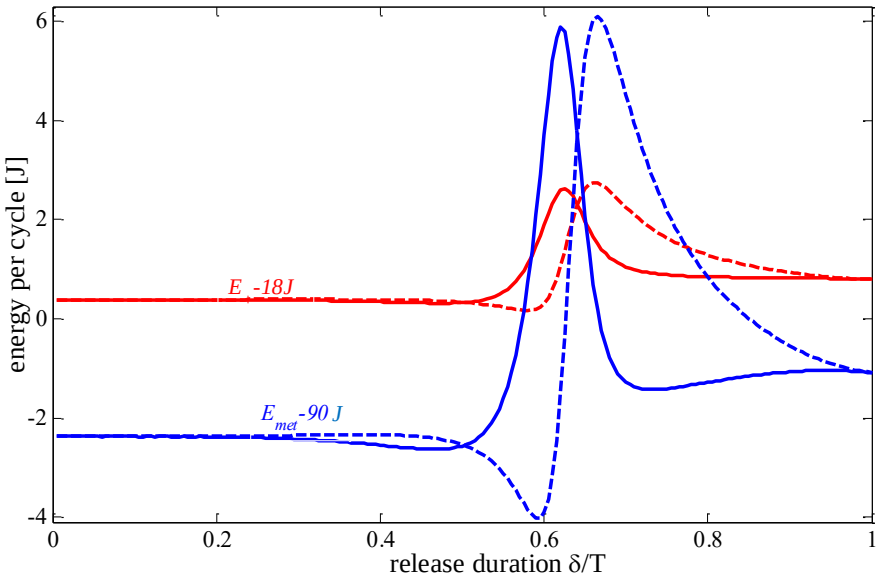

Figure 13: Plot of energy expenditure E as a function of δ/T for $\varphi=0.6T$ under the timing-based switching law.

4.2 Combined optimization of suspension stiffness and clutch timing

We now investigate the influence of the suspension stiffness k_2 on energy expenditure and amplitude of oscillations. The stiffness k_2 is varied within the range $200-5500\left[N/m\right]$ while the damping coefficient c_2 is chosen such that the dimensionless damping ratio, defined as $\zeta = \frac{c_2}{2\sqrt{m_2 k_2}}$, is kept constant as ζ=0.025. We consider two cases, where the first case involves a free spring without locking (equivalent to $\delta=T$). The second case involves optimal switching time under the event-based switching law, as discussed above. Figure 14 plots the energy expenditure E as a function of the suspension stiffness k_2, where the dashed line corresponds to the case of a free spring while the solid line denotes E under the optimal switching times of the clutch. The plot clearly indicates that the optimal stiffness which minimizes the energy expenditure is $k^* \approx 1600 N/m$. Moreover, for $k_2 \leq k^*$, the energy is minimized without switching, i.e. at $\delta=T$. On the other hand, for $k_2 > k^*$, the energy expenditure under a free spring rises sharply, and can be significantly reduced by using the clutch with optimal timing. The rightmost dash-dotted vertical line corresponds to the nominal value of k_2=5147N/m which is considered here and in [11],[14]. The energy expenditure with and without optimal clutch timing are precisely the ones that appear in Figure 9 (minimum point and right endpoint of $\delta \to T$). It can be seen that the energy expenditure under this value of k_2 without clutch timing is larger than the case of rigid connection $k \to \infty$ (denoted by the dotted horizontal line), and that clutch timing can significantly reduce the energetic cost. The leftmost dash-dotted vertical line corresponds to the value k_2=530N/m of the suspension system studied experimentally in [12]. It can be seen that this value is closer to the optimal point, where energy cost is minimized without the need for clutch timing. It is important to note that the choice of optimal stiffness k_2 is specific to a given backpack mass m_2 and walking speed, which also affects the leg oscillation frequency ω [27]. Therefore, if the optimal spring k_2 is chosen for specific conditions, then when the system encounters a significant change in its conditions for which the chosen stiffness becomes sub-optimal, the energy expenditure can then be minimized by tuning the clutch timing parameters without the need to change the suspension system. Finally, we computed the oscillation amplitude of the suspension system Δz along the periodic solution, which is defined as $\Delta z = \max_t \left\{ z_2(t) - z_1(t) \right\} - \min_t \left\{ z_2(t) - z_1(t) \right\}$. Figure 15 plots Δz as a function of suspension stiffness k_2, where the damping ratio ζ is kept constant and all other physical parameters are chosen as in Table 1. The solid line is for the energy-optimal choice of clutch timing, while the dashed line is for a free spring without a clutch. It can be seen that the energy-optimal choice of clutch timing parameter also results in a significant reduction in the oscillation amplitude of the suspension system, which is a significant factor in the comfort feeling of the human carrying the load.

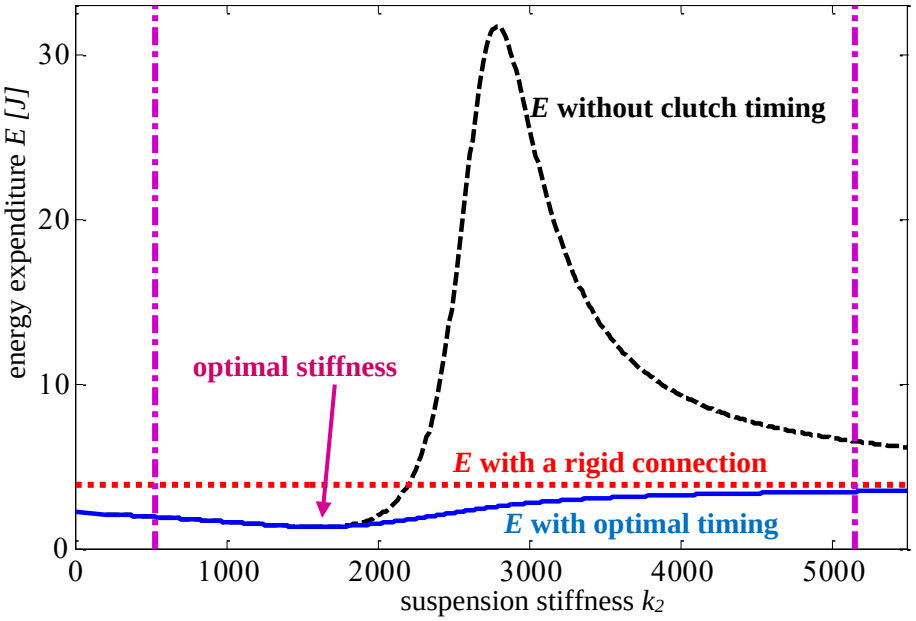

Figure 14: Plot of energy expenditure *E* vs. suspension stiffness k_2.

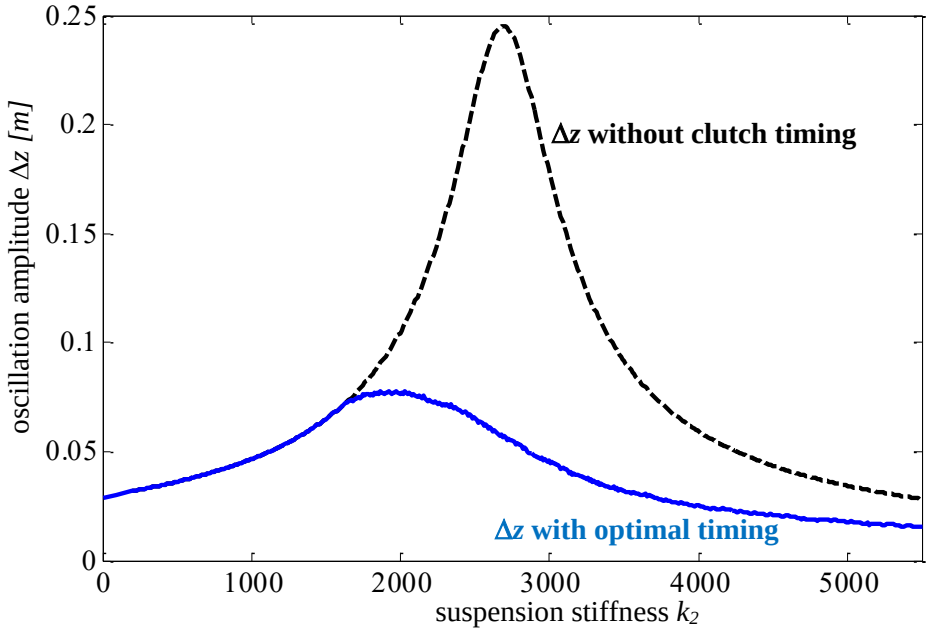

Figure 15: Plot of oscillation amplitude Δz vs. suspension stiffness k_2.

Finally, we study the influence of suspension stiffness and clutch timing on the load force that the backpack exerts on the body. This force is given by:

$$f_{load}(t) = m_2\left(\ddot{z}_2(t) + g\right). \tag{27}$$

As an example, Figure 15 plots the load force as a function of time for a the steady-state periodic solution under the nominal suspension stiffness k_2=5147 *N/m*. The dashed curve is load force for a fully active spring without clutch locking (δ=*T*), which is oscillating harmonically about the mean value of $m_2 g$, shown in dotted

horizontal line. The solid curve is the load force under the energy-optimal clutch timing of $\delta=0.499T$ with event-based switching law. The discontinuities in the load force occur at the times of releasing and locking the clutch.

When the suspension stiffness is varied, Figure 17 plots the maximal and minimal load forces under fully active spring ($\delta=T$) in dashed curve, and under energy-optimal event-based clutch timing in solid curve. Below the optimal stiffness $k_2 \leq k^*$, the two curves coincide since the best switching is at $\delta=T$ for this range. The dotted horizontal lines correspond to a fully locked connection ($\delta=0$). The curves of minimal and maximal forces under $\delta=0$ and $\delta=T$ are symmetric with respect to the mean value of $m_2 g$ (dash-dotted horizontal line), whereas the curves under optimal clutch timing are not precisely symmetric, as illustrated in Figure 16. It can be seen that for large suspension stiffness $k_2 > k^*$, optimal clutch timing results in significant reduction in the oscillation amplitude of the load force. In addition, for a fully active spring ($\delta=T$) the amplitude peak at $k_2 \approx 2500$ appears both in the load force (Figure 17) and the oscillation amplitude Δz (Figure 15). This indicates that energy efficiency is strongly correlated with reduction in amplitudes of both the load force and oscillations Δz.

5. Conclusion

In this work, we theoretically studied the incorporation of a timed clutch mechanism into an elastic backpack suspension system. We used the simple two-mass model studied in [14] and extended it in order to account for the hybrid dynamics induced by clutch transitions between states of a rigid constraint and a spring-damper connection. We analyzed periodic solutions and their stability under timing-based

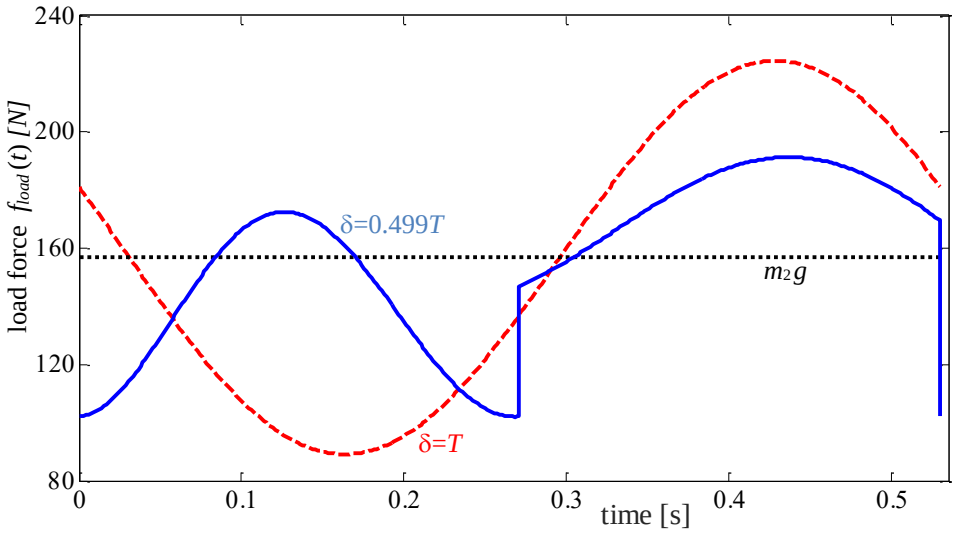

Figure 16: Plot of the load force f_{load}(t) during periodic solutions. Dashed line – fully active spring ($\delta=T$), solid line – event-based clutch timing of $\delta=0.499T$.

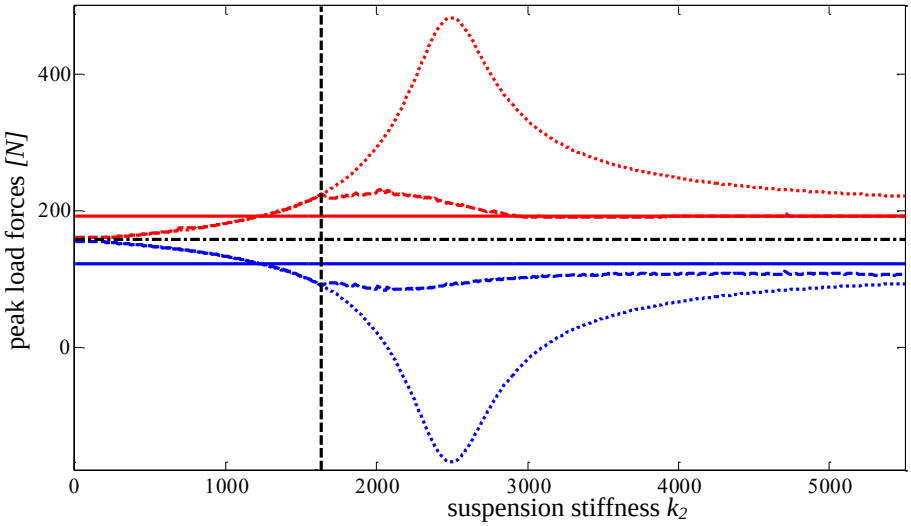

Figure 17: Minimal and maximal load forces as a function of suspension stiffness k_2. Dashed line – fully active spring ($\delta=T$), solid line – event-based clutch timing, dotted line – fully locked connection $\delta=0$.

and event-based switching laws of the clutch, and computed the resulting energy expenditure. We have found optimal combinations of clutch timing and suspension stiffness that minimize energy expenditure. It has been found that for given conditions of walking speed and load, an optimal stiffness can be obtained that minimizes energy expenditure without the need for clutch locking. Nevertheless, if the chosen spring is sub-optimal or the walking conditions have changed, the optimal choices of clutch timing can significantly reduce the energetic cost and attenuate the amplitudes of backpack oscillations and loading force. These theoretical results indicate that incorporating mechanical clutch elements into backpack suspension systems can have a promising potential for improving the system's performance and user's comfort.

We now briefly discuss some limitations of the current analysis and list future directions for possible extensions of the research. First, the two-mass model studied here following [14], which accounts only for vertical motion, is obviously an over-simplification. A more detailed model should be at least planar, and must account for the full joint kinematics of the legs and lower back during normal and loaded walking gait. In this context, it is worth exploring optimization of the event-driven clutch timing for the passive wearable device of Collins *et al* [19], and examine other choices of triggering events with biomechanical relevance, such as knee lock, foot touchdown, etc. Second, any mechanical design of a clutch-based backpack suspension system in practice must consider the details of the mechanism for clutch locking and disengagement. This mechanism can either be purely mechanical, using cam-shafts, springs and/or a ratchet and pawl as in [19],[20], or it may include electrical actuation that applies mechanical brakes, making it only a *semi-passive* mechanism [17],[18],[22]. The design of clutch-based backpack suspension systems must also account for practical and ergonomic considerations such as weight, size, user comfort and manufacturing constraints. Additionally, any practical assessment of backpack suspension system's performance must rely on

measurements of metabolic energy consumption under experimental trials on human subjects. Finally, it might prove useful to investigate the incorporation of timed clutches into other applications of load suspension systems such as handle mechanisms [36],[37], as well as legged robots [38].

Acknowledgement:

This research has been supported by The Israeli Ministry of Defense (MAFAT), under Technion grant no. 2021907. We thank the anonymous reviewers for helpful comments and suggestions.

References:

[1] Knapik, J. J., Reynolds, K. L., & Harman, E. (2004). Soldier load carriage: historical, physiological, biomechanical, and medical aspects. Military medicine, 169(1), 45.

[2] Maloiy, G. M. O., Heglund, N. C., Prager, L. M., Cavagna, G. A., & Taylor, C. R. (1986). Energetic cost of carrying loads: have African women discovered an economic way?. Nature 319, 668-669.

[3] Bastien, G. J., Schepens, B., Willems, P. A., & Heglund, N. C. (2005). Energetics of load carrying in Nepalese porters. Science, 308(5729), 1755-1755.

[4] Ren, L., Jones, R. K., & Howard, D. (2005). Dynamic analysis of load carriage biomechanics during level walking. Journal of biomechanics, 38(4), 853-863.

[5] Knapik, J., Harman, E., & Reynolds, K. (1996). Load carriage using packs: a review of physiological, biomechanical and medical aspects. Applied ergonomics, 27(3), 207-216.

[6] Keren, G., Epstein, Y., Magazanik, A., & Sohar, E. (1981). The energy cost of walking and running with and without a backpack load. European Journal of Applied Physiology and occupational physiology, 46(3), 317-324.

[7] Bastien, G. J., Willems, P. A., Schepens, B., & Heglund, N. C. (2005). Effect of load and speed on the energetic cost of human walking. European Journal of Applied Physiology, 94(1-2), 76-83.

[8] Kenntner, G. (1969). Gebräuche und Leistungsfähigkeit im Tragen von Lasten bei Bewohnern des südlichen Himalaya: Ein Beitrag zur biogeographischen Forschung. Zeitschrift für Morphologie und Anthropologie, (H. 2), 125-169.

[9] Kram, R. (1991). Carrying loads with springy poles. Journal of Applied Physiology, 71(3), 1119-1122.

[10] Alexander, R. M. (1988). Elastic mechanisms in animal movement. Cambridge University Press.

[11] Foissac, M., Millet, G. Y., Geyssant, A., Freychat, P., & Belli, A. (2009). Characterization of the mechanical properties of backpacks and their influence on the energetics of walking. Journal of biomechanics, 42(2), 125-130.

[12] Rome, L. C., Flynn, L., & Yoo, T. D. (2006). Biomechanics: Rubber bands reduce the cost of carrying loads. Nature, 444(7122), 1023-1024.

[13] Hoover, J., & Meguid, S. A. (2011). Performance assessment of the suspended-load backpack. International Journal of Mechanics and Materials in Design, 7(2), 111-121.

[14] Ackerman, J., & Seipel, J. (2014). A model of human walking energetics with an elastically-suspended load. Journal of biomechanics, 47(8), 1922-1927.

[15] Alexander, R. (1990). Three uses for springs in legged locomotion. International Journal of Robotics Research, 9(2), 53-61.

[16] Bauer, F., Römer, U., Fidlin, A., & Seemann, W. (2016). Optimization of energy efficiency of walking bipedal robots by use of elastic couplings in the form of mechanical springs. Nonlinear Dynamics, 83(3), 1275-1301.

[17] Dollar, A. M., & Herr, H. (2008, September). Design of a quasi-passive knee exoskeleton to assist running. In Intelligent Robots and Systems, 2008. IROS 2008. IEEE/RSJ International Conference on (pp. 747-754). IEEE.

[18] Walsh, C. J., Endo, K., & Herr, H. (2007). A quasi-passive leg exoskeleton for load-carrying augmentation. International Journal of Humanoid Robotics, 4(03), 487-506.
[19] Collins, S. H., Wiggin, M. B., & Sawicki, G. S. (2015). Reducing the energy cost of human walking using an unpowered exoskeleton. Nature, 522(7555), 212-215.
[20] Wiggin, M. B., Sawicki, G. S., & Collins, S. H. (2011, June). An exoskeleton using controlled energy storage and release to aid ankle propulsion. In Rehabilitation Robotics (ICORR), 2011 IEEE International Conference on (pp. 1-5). IEEE.
[21] Rouse, E. J., Mooney, L. M., Martinez-Villalpando, E. C., & Herr, H. M. (2013, June). Clutchable series-elastic actuator: Design of a robotic knee prosthesis for minimum energy consumption. In Rehabilitation Robotics (ICORR), 2013 IEEE International Conference on (pp. 1-6). IEEE.
[22] Torrealba, R. R., Udelman, S. B., & Fonseca-Rojas, E. D. (2017). Design of variable impedance actuator for knee joint of a portable human gait rehabilitation exoskeleton. Mechanism and Machine Theory, 116, 248-261.
[23] Paluska, D., & Herr, H. (2006). The effect of series elasticity on actuator power and work output: Implications for robotic and prosthetic joint design. Robotics and Autonomous Systems, 54(8), 667-673.
[24] Häufle, D. F., Taylor, M. D., Schmitt, S., & Geyer, H. (2012, June). A clutched parallel elastic actuator concept: Towards energy efficient powered legs in prosthetics and robotics. In Biomedical Robotics and Biomechatronics (BioRob), 2012 4th IEEE RAS & EMBS International Conference on (pp. 1614-1619). IEEE.
[25] Williams, R. J., Hansen, A. H., & Gard, S. A. (2009). Prosthetic ankle-foot mechanism capable of automatic adaptation to the walking surface. Journal of biomechanical engineering, 131(3), 035002.
[26] Zhang, L., Xu, D., Makhsous, M., & Lin, F. (2000). Stiffness and viscous damping of the human leg. In Proc. of the 24th Ann. Meeting of the Am. Soc. of Biomech., Chicago, IL.
[27] Grieve, D. W., & Gear, R. J. (1966). The relationships between length of stride, step frequency, time of swing and speed of walking for children and adults. Ergonomics, 9(5), 379-399.
[28] Kailath, T. (1980). Linear systems (Vol. 156). Englewood Cliffs, NJ: Prentice-Hall.
[29] Guckenheimer, J., & Holmes, P. J. (2013). Nonlinear oscillations, dynamical systems, and bifurcations of vector fields (Vol. 42). Springer Science & Business Media.
[30] Lax, P. D. (2002). Functional Analysis (Pure and Applied Mathematics: A Wiley-Interscience Series of Texts, Monographs and Tracts).
[31] Bernardo, M., Budd, C., Champneys, A. R., & Kowalczyk, P. (2008). Piecewise-smooth dynamical systems: theory and applications (Vol. 163). Springer Science & Business Media.
[32] Wendel, E., & Ames, A. D. (2012). Rank deficiency and superstability of hybrid systems. Nonlinear Analysis: Hybrid Systems, 6(2), 787-805.
[33] Ackerman, J., & Seipel, J. (2016). Effects of independently altering body weight and mass on the energetic cost of a human running model. Journal of biomechanics, 49(5), 691-697.
[34] Li, D., Li, T., Li, Q., Liu, T., & Yi, J. (2016). A simple model for predicting walking energetics with elastically-suspended backpack. J. of biomechanics, 49(16), 4150-4153.
[35] Margaria, R. (1976). Biomechanics and energetics of muscular exercise. Oxford University Press, USA.
[36] Ackerman, J., Kelley, K., & Seipel, J. (2015). Dynamics of carrying a load with a handle suspension. Journal of biomechanics, 48(6), 1084-1091.
[37] Ackerman, J., & Seipel, J. (2015). Design of stabilizing arm mechanisms for carrying and positioning loads. Journal of Mechanical Design, 137(10), 104501.
[38] Ackerman, J., & Seipel, J. (2013). Energy efficiency of legged robot locomotion with elastically suspended loads. IEEE Transactions on Robotics, 29(2), 321-330.